

## Terahertz spectroscopy of gelatin-embedded human brain gliomas of different grades: a road toward intraoperative THz diagnosis

Arseniy A. Gavdush  
Nikita V. Chernomyrdin  
Kirill M. Malakhov  
Sheyh-Islyam T. Beshplav  
Irina N. Dolganova  
Alexandra V. Kosyrkova  
Pavel V. Nikitin  
Guzel R. Musina  
Gleb M. Katyba  
Igor V. Reshetov  
Olga P. Cherkasova  
Gennady A. Komandin  
Valery E. Karasik  
Alexander A. Potapov  
Valery V. Tuchin  
Kirill I. Zaytsev

Arseniy A. Gavdush, Nikita V. Chernomyrdin, Kirill M. Malakhov, Sheyh-Islyam T. Beshplav, Irina N. Dolganova, Alexandra V. Kosyrkova, Pavel V. Nikitin, Guzel R. Musina, Gleb M. Katyba, Igor V. Reshetov, Olga P. Cherkasova, Gennady A. Komandin, Valery E. Karasik, Alexander A. Potapov, Valery V. Tuchin, Kirill I. Zaytsev, "Terahertz spectroscopy of gelatin-embedded human brain gliomas of different grades: a road toward intraoperative THz diagnosis," *J. Biomed. Opt.* **24**(2), 027001 (2019), doi: 10.1117/1.JBO.24.2.027001.

# Terahertz spectroscopy of gelatin-embedded human brain gliomas of different grades: a road toward intraoperative THz diagnosis

Arseniy A. Gavdush,<sup>a,b</sup> Nikita V. Chernomyrdin,<sup>a,b</sup> Kirill M. Malakhov,<sup>a,b</sup> Sheyh-Islyam T. Beshplav,<sup>c</sup> Irina N. Dolganova,<sup>b,d</sup> Alexandra V. Kosyrkova,<sup>c</sup> Pavel V. Nikitin,<sup>c</sup> Guzel R. Musina,<sup>a,b</sup> Gleb M. Katyba,<sup>b,d</sup> Igor V. Reshetov,<sup>e</sup> Olga P. Cherkasova,<sup>a,f</sup> Gennady A. Komandin,<sup>a</sup> Valery E. Karasik,<sup>b</sup> Alexander A. Potapov,<sup>c</sup> Valery V. Tuchin,<sup>g</sup> and Kirill I. Zaytsev<sup>a,b,\*</sup>

<sup>a</sup>Prokhorov General Physics Institute of the Russian Academy of Sciences, Moscow, Russia

<sup>b</sup>Bauman Moscow State Technical University, Moscow, Russia

<sup>c</sup>Burdenko Neurosurgery Institute, Moscow, Russia

<sup>d</sup>Institute of Solid State Physics of the Russian Academy of Sciences, Chernogolovka, Russia

<sup>e</sup>Sechenov First Moscow State Medical University, Institute of Regenerative Medicine, Moscow, Russia

<sup>f</sup>Institute of Laser Physics of the Siberian Branch of the Russian Academy of Sciences, Novosibirsk, Russia

<sup>g</sup>Saratov State University, Saratov, Russia

**Abstract.** We applied terahertz (THz)-pulsed spectroscopy to study *ex vivo* the refractive index and absorption coefficient of human brain gliomas featuring different grades, as well as perifocal regions containing both intact and edematous tissues. Glioma samples from 26 patients were considered and analyzed according to further histological examination. In order to fix tissues for the THz measurements, we applied gelatin embedding, which allows for sustaining their THz response unaltered, as compared to that of the freshly excised tissues. We observed a statistical difference between the THz optical constants of intact tissues and gliomas of grades I to IV, while the response of edema was similar to that of tumor. The results of this paper justify a potential of THz technology in the intraoperative label-free diagnosis of human brain gliomas for ensuring the gross-total resection. © The Authors. Published by SPIE under a Creative Commons Attribution 4.0 Unported License. Distribution or reproduction of this work in whole or in part requires full attribution of the original publication, including its DOI. [DOI: 10.1117/1.JBO.24.2.027001]

Keywords: terahertz technology; terahertz-pulsed spectroscopy; human brain gliomas; terahertz optical properties; refractive index; absorption coefficient; intraoperative neurodiagnosis; gelatin embedding.

Paper 180633LR received Nov. 26, 2018; accepted for publication Jan. 11, 2019; published online Feb. 6, 2019.

Gliomas form the most common type of primary brain tumors, representing about 26% of all primary tumors and 81% of malignant primary tumors of the brain.<sup>1</sup> Malignant gliomas, especially glioblastoma, have a poor prognosis and a bad patient outcome, even when applying an aggressive therapy.<sup>2</sup> Among the prognostic factor of glioma treatment, achievement of its gross-total resection is a crucial one for reducing the probability of tumor recurrence and increasing the patients' survival.<sup>3</sup> At the same time, gliomas usually possess unclear margins, complicating their gross-total resection.<sup>4</sup> Nowadays, several techniques of intraoperative neurodiagnosis are rapidly developed or already applied in clinical practice.<sup>5</sup> Among them, we would particularly mention intraoperative magnetic resonance imaging,<sup>6</sup> fluorescence spectroscopy and imaging relying on fluorescence of protoporphyrin IX, induced by 5-aminolevulinic acid (5-ALA),<sup>7</sup> or fluorescein sodium,<sup>8</sup> Raman spectroscopy and imaging,<sup>9</sup> photoacoustic imaging,<sup>10</sup> optical coherence tomography,<sup>11</sup> etc. Nevertheless, existing techniques fail to address all demanding problems of the intraoperative diagnosis of human brain gliomas, justifying an importance of further development of instruments for the intraoperative brain tumor diagnosis.

Most recently, terahertz (THz) spectroscopy and imaging have attracted significant attention as promising methods for the intraoperative neurodiagnosis.<sup>12</sup> During the past decades,

THz technology has been rapidly developed<sup>13,14</sup> and applied in the label-free diagnosis of malignancies with different nosology and localization.<sup>12</sup> They provide an ability for sensing the picosecond relaxation dynamics in tissues,<sup>15</sup> the tissue probing depth of about hundreds of microns,<sup>12</sup> and the sub-millimeter-scale spatial resolution.<sup>16</sup> In Ref. 17, a pilot study of the tumor models in a whole brain from a rat using THz imaging has been performed, revealing a contrast between normal tissues and orthotopic glioma model for both the freshly excised and paraffin-embedded tissues. These differences were attributed to increased water content in a tumor (owing to the newly generated blood vessels and the body fluids around necrotic debris<sup>18</sup>) and changes of cell density in a tumor. Furthermore, in this paper, a contrast between the gray and white matter of the brain has been observed in the THz images, reportedly originating from higher content of myelin in the white matter. In Ref. 19, analysis of paraffin-embedded brain glioma models from mice has been carried out using the THz-pulsed spectroscopy. It reveals optimal spectral bands and features for the differentiation between healthy tissues and tumors of the brain. In Refs. 20–22, a potential of the THz reflectometry and imaging in the intraoperative neurodiagnosis have been highlighted involving glioma models from mice and rats, both *ex vivo* and *in vivo*, as well as few samples of human brain gliomas *ex vivo*. Thereby, the attractiveness of THz technology in intraoperative diagnosis of brain tumors has been demonstrated in several pilot papers by studying predominantly tumor models from mice and rats. Nevertheless, a comprehensive analysis

\*Address all correspondence to Kirill I. Zaytsev, E-mail: kirzay@gmail.com

of brain tumors from humans is required in order to objectively uncover strengths and weaknesses of THz technology in the intraoperative diagnosis of human brain gliomas.

In order to address this problem, in this work, we study the THz refractive index and absorption coefficient of *ex vivo* human brain gliomas, featuring different World Health Organization (WHO) grades, and perifocal regions comprised of intact (healthy) and edematous tissues. The tissue specimens were excised according to the preliminary medical diagnosis, covered by gelatin slabs,<sup>23</sup> and characterized using the reflection-mode THz-pulsed spectroscopy and the hematoxylin and

eosin (H&E)-stained histology. Analysis of the experimental data reveals statistical differences between the THz response of intact tissues in the perifocal region and gliomas of WHO grades I to IV, which are caused by the endogenous markers. Meanwhile, the THz optical constants of edema in the perifocal region differ from that of intact tissues, being closer to that of tumors. Thereby, the results of this study justify a prospect of THz technology in the intraoperative label-free diagnosis of both low and high grade gliomas of the human brain.

In Table 1, we show the information about 26 samples of human brain gliomas *ex vivo*, provided by Burdenko Neurosurgery Institute and classified by WHO grade;<sup>1</sup> among them, 2, 9, 4, and 11 gliomas of grades I, II, III, and IV, respectively. Along with the tumor, the samples contained perifocal regions, comprised of intact and edematous tissues and featuring rather small dimensions; therefore, the diffraction-limited resolution of our THz optical system yielded characterization of perifocal region from six samples. After resection, the tissue specimens were placed onto a substrate and covered by a gelatin slab for the THz measurements.<sup>22</sup> The gelatin embedding of tissues allowed for preventing them from hydration/dehydration; thus, sustaining their THz response unaltered for several hours, as compared to that of freshly excised tissues.<sup>23</sup> Finally, a routine H&E-stained histology was applied to confirm the diagnosis.

For the THz measurements of brain tissues, we used the THz-pulsed spectrometer operating in a reflection mode; it was described in details in Refs. 22 and 24. We notice that it is equipped with a unit for the reflection-mode measurements, based on a pair of gold-coated off-axis parabolic mirrors and a quartz window, on the top of which the tissue sample is handled [Fig. 1(a)]. The THz beam irradiating the sample is *s*-polarized. The focusing mirror features the focal length of  $f = 50$  mm and the diameter of  $D = 25$  mm. Assuming the diffraction-limited character of the focusing system, we could estimate the Airy disc radius at the focal plane, which gives us the Rayleigh resolution limit

$$r = \frac{1.22\lambda f}{Dn_{\text{SiO}_2}} \equiv 1.14\lambda, \quad (1)$$

where  $n_{\text{SiO}_2} \approx 2.150$  stands for the refractive index of reference quartz window. Evidently, the spatial resolution of the focusing system and the area of tissue surface, from which the signal is collected, depend on  $\lambda$  and decrease with increasing frequency. At the same time, the tissue probing depth (i.e., the depth of THz wave amplitude penetration into tissues) is inversely proportional to the frequency-dependent amplitude absorption coefficient,  $\delta = 1/\alpha$ . It depends both on the considered type of tissues and on the electromagnetic frequency and usually has a value of hundreds of microns in the THz band. The volume of tissues, which is probed during our THz measurements, varies with frequency and could be estimated as  $V = \pi r^2 \delta$ . The experimental setup is covered by the plastic housing and purged with the nitrogen gas for suppressing an impact of water vapors on the THz measurements.

In order to objectively compare the THz responses of healthy and pathological tissues, we reconstructed their THz refractive index  $n$  and amplitude absorption coefficient  $\alpha$  in the spectral range of about  $\nu = 0.2$  to 1.5 THz. These physical characteristics are related to the complex refractive index

**Table 1** Information about human glioma samples.

#	Age	Gender	Pathology	WHO grade
1	39	Female	Piloid astrocytoma	I
2	25	Female	Gangliocytoma	I
3	31	Male	Diffuse astrocytoma	II
4	56	Female	Oligodendroglioma	II
5	29	Male	Diffuse astrocytoma	II
6	42	Male	Diffuse astrocytoma	II
7	34	Female	Oligodendroglioma	II
8	43	Male	Oligodendroglioma	II
9	18	Male	Pleomorphic xanthoastrocytoma	II
10	63	Female	Diffuse astrocytoma	II
11	58	Female	Oligodendroglioma	II
12	47	Female	Anaplastic astrocytoma	III
13	26	Female	Anaplastic oligodendroglioma	III
14	68	Male	Anaplastic oligodendroglioma	III
15	38	Male	Anaplastic oligodendroglioma	III
16	35	Male	Glioblastoma	IV
17	63	Female	Glioblastoma	IV
18	34	Female	Glioblastoma	IV
19	56	Male	Glioblastoma	IV
20	55	Female	Glioblastoma	IV
21	54	Female	Glioblastoma	IV
22	69	Female	Glioblastoma	IV
23	64	Female	Glioblastoma	IV
24	54	Female	Glioblastoma	IV
25	50	Male	Gliosarcoma	IV
26	55	Female	Glioblastoma	IV

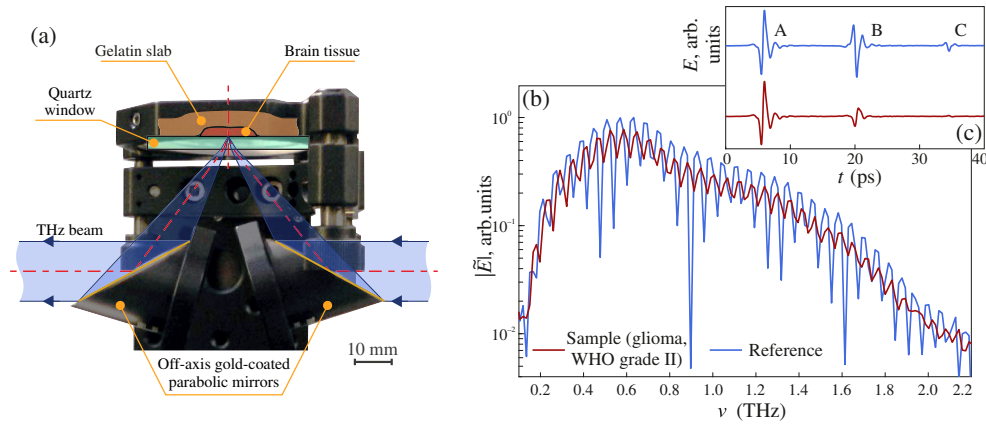


**Fig. 1** Experimental characterization of gelatin-embedded human brain gliomas: (a) a reflection-mode THz spectroscopy unit, based on off-axis gold-coated parabolic mirrors and a reference window, on the top of which the tissue sample is handled; (b), (c) reference  $E_r$  and sample  $E_s$  signals of the THz-pulsed spectrometer, represented in the frequency and time domains, respectively. In (a), the angle of THz wave incidence on the quartz window–tissue (or free space) interface is  $\theta \simeq 17$  deg.

$$\tilde{n} = n - i \frac{c_0}{2\pi\nu} \alpha, \quad (2)$$

where  $c_0 \simeq 3 \times 10^8$  m/s is the speed of light in a free space; they do not depend on the method of measurements and completely describe the THz wave–tissue interaction in the framework of classical electrodynamics.<sup>15</sup>

From Figs. 1(b) and 1(c), we notice that two signals of the THz-pulsed spectrometer are used for reconstruction of  $n$  and  $\alpha$ —the reference  $E_r$  and sample  $E_s$  ones, reflected from the empty quartz window and the quartz window with the tissue sample behind, correspondingly. From Fig. 1(c), we notice that both reference and sample waveforms are comprised of three separate wavelets, labeled as A, B, and C. The wavelets A and B correspond to THz wave reflection from the free space–quartz and quartz–tissue (or quartz–free space) interfaces, respectively, while C represents the satellite pulse caused by the multiple THz wave reflection in the quartz window. Notice, the wavelet A is equal for both reference and sample waveforms. As shown in Fig. 1(b), these three wavelets form an interference pattern in the frequency domain.

Prior to reconstruction of the optical properties, we applied the apodization procedure to both the reference and sample waveforms—namely, the 20-ps-width fourth-term Blackman–Harris window filter,<sup>25</sup> centered at the peak of the wavelet B. This filter provides the frequency-domain resolution of  $\Delta\nu \simeq 0.05$  THz and allows for filtering out a contribution of the wavelets A and C. Then, we defined the frequency-domain B-wavelet-based experimental and theoretical transfer functions:

$$\tilde{H}_{\text{exp}} = \frac{\tilde{E}_s}{\tilde{E}_r}, \quad \tilde{H}_{\text{th}} = \frac{\tilde{R}_{23}}{\tilde{R}_{21}}, \quad (3)$$

which depend on the Fresnel reflection of  $s$ -polarized THz wave at the quartz–tissue (or free space) interface

$$\tilde{R}_{\text{mk}} = \frac{\tilde{n}_m \cos(\theta_i) - \tilde{n}_k \cos(\theta_t)}{\tilde{n}_m \cos(\theta_i) + \tilde{n}_k \cos(\theta_t)}, \quad (4)$$

here, indexes  $m, k = 1, 2$ , and 3 correspond to the free space, quartz, and tissue,  $\theta_i$  and  $\theta_t$  define the angles of incidence and

transmittance. Finally, we determined the complex refractive index of tissues  $\tilde{n}_3$  via minimization of the vector error functional:

$$\tilde{n}_3 = \text{argmin}_{\tilde{n}_3} [\Phi], \quad \Phi = \left( \begin{array}{l} \|\tilde{H}_{\text{exp}} - \tilde{H}_{\text{th}}\| \\ |\phi[\tilde{H}_{\text{exp}}] - \phi[\tilde{H}_{\text{th}}]| \end{array} \right), \quad (5)$$

where  $\|\dots\|$  and  $\phi[\dots]$  are operators allowing to extract modulus and phase of a complex value.

In Fig. 2, we demonstrate  $n$  and  $\alpha$ , observed for the studied tissues, as well as representative data of the H&E-stained histology. For each tissue specimen, we examined the reproducibility of the experimental data and the fluctuations of  $n$  and  $\alpha$  by measuring different points of the sample surface. By analyzing the data of these spatially resolved measurements, we found that the THz response of perifocal region splits into two distinct classes, which are supposed to be attributed to the intact and edematous tissues. Therefore, in Fig. 2, we show mean values and error bars for  $n$  and  $\alpha$  corresponding to the intact tissues, edema, and gliomas of grades I to IV, where the error bars represent the  $\pm 2.0\sigma$  ( $\simeq 95\%$ ) confidential intervals;  $\sigma$  is the standard deviation. We performed the Kolmogorov–Smirnov test, which revealed normal character of statistical distributions, formed by each distinct class of tissues. In complete accordance with the results from Refs. 17–22, we observed statistical difference between the intact tissues and tumors, as well as the intact tissues and edematous tissues. Particularly, the refractive index of all gliomas and edematous tissues is higher than that of intact tissues. The observed label-free contrast of several percentages between the intact tissues and tumor agrees with the results from Ref. 21. In addition, we performed a two-sample  $p$ -value test for various types of tissues considering their refractive index at 1.0 THz. The observed  $p$ -values provided an evidence of a difference between the mean values of the intact tissue and gliomas of all grades, as well as the intact tissues and the edematous tissues; for these pairs of tissue classes, the  $p$ -values are smaller than the selected significance value, i.e.,  $p < 10^{-3}$ . In turn, the  $p$ -value test did not show difference between the mean values of edematous tissues and gliomas of all grades, i.e.,  $p > 10^{-3}$ . Thus, our experimental data allow for concluding that we are unable to discriminate edematous tissues from tumors and to differentiate between gliomas of various WHO grades.

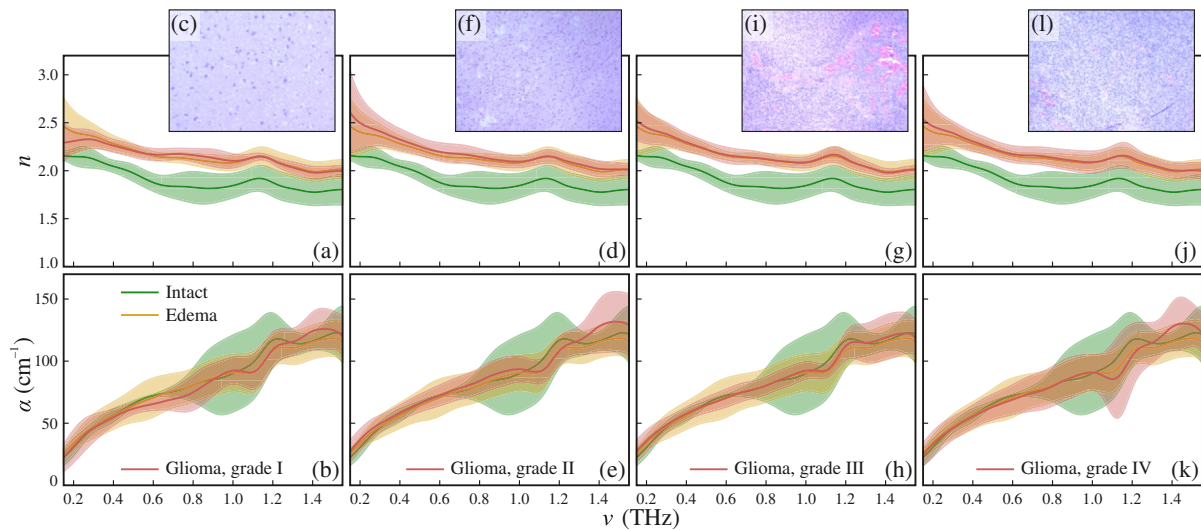


**Fig. 2** Refractive index  $n$ , amplitude absorption coefficient  $\alpha$ , and H&E-stained histology of gelatin-embedded human brain gliomas of different WHO grades *ex vivo*: (a)–(c) grade I; (d)–(f) grade II; (g)–(i) grade III; and (j)–(l) grade IV. The THz optical properties of gliomas are compared with equal data for the intact and edematous tissues, averages within the entire set of brain tissues specimens. The error bars represent a  $\pm 2.0\sigma$  confidential interval of measurements, assuming fluctuation of optical properties within each tissue sample and each tissue class.

In Fig. 2, significant dispersion of optical properties is observed for each tissue class, that is, usual for majority of the label-free spectroscopy and imaging modalities.<sup>12</sup> High dispersion of experimental curves might be attributed to heterogeneous character of tissues. Particularly, we did not differentiate intact brain tissues into the white and gray matter, which might be the reason of higher dispersion for this class of tissues. In turn, the dispersion of glioblastoma (glioma, grade IV) response could originate owing to the presence of tissue inhomogeneities caused by necrotic debris, which is specifically inherent to glioblastoma. Such an inhomogeneous character of tissues at THz frequencies might be specific for various types of human brain tumors, forming a subject of additional comprehensive research work, for example, using modern methods of high-resolution THz microscopy.<sup>12,16</sup> At the same time, nonmonotonic character and increased dispersion of the experimental data at the frequencies above 0.8 THz should not be attributed to the THz optical properties of biological tissues, which usually possess no resonant features.<sup>15</sup> They might be due to measurement errors originating from fluctuations of humidity along the THz beam path and from the drop of the THz-pulsed spectrometer signal [see Fig. 1(b)]. Finally, an increasing dispersion of experimental data at frequencies below 0.3 THz might be due to the limited resolution of our THz optical system [see Eq. (1)] and, also, to the drop of the THz-pulsed spectrometer signal [see Fig. 1(b)].

The use of the gelatin embedding of tissues *ex vivo* makes our THz measurement of fixed tissues close to that of freshly excised tissues. Nevertheless, we are not able to reproduce blood flow in environment *in vivo*, which certainly has a lot of water and other components. The results of our study confirmed the earlier-reported differences between intact tissues and tumors of the brain, which were demonstrated predominantly using glioma models from mice and rats,<sup>17–21</sup> generalizing capabilities of the THz technology to the intraoperative diagnosis of brain gliomas in humans. Namely, the THz spectroscopy and imaging could become instruments for the

label-free delineation of glioma margins during surgery, ensuring the gross-total resection. As reported in Ref. 22, a contrast between the THz response of intact tissues and tumor is also observed for that types of human brain gliomas, which are less-effectively diagnosed by the 5-ALA-induced fluorescence spectroscopy and imaging. This highlights the potential advantage of the THz diagnosis over this well-known modality of the intraoperative brain spectroscopy and imaging.

The observed contrast between the gelatin-embedded intact tissues and gliomas is due to the increased water content in tumor, caused by the abnormal vascularity and edema.<sup>17</sup> In turn, other biological events, such as increase of the cell density and changes in the protein concentration in a tumor, also contribute to the contrast, but their contribution is reportedly several times smaller than that of changes in water content.<sup>17</sup> When using THz spectroscopy and imaging for the intraoperative delineation of glioma margins, the edematous tissues in the perifocal region may be confused with tumor, similarly to the false-positive results, occurring during the intraoperative THz diagnosis of nonmelanoma skin cancers.<sup>26,27</sup> Recently, an ability to use the THz technology in diagnosis of different degrees of traumatic brain injury has been demonstrated owing to different water content and spatial distribution of hematoma components in normal and injured tissues of the brain.<sup>28,29</sup> Therefore, we might also expect fault positive results of THz diagnosis of brain tumor in presence of traumatic brain injury. A prospective approach to mitigate this difficulty is associated with a combination of THz diagnosis with other label-free imaging modalities.<sup>12</sup>

We should mention that we assumed the tissues of the brain to be homogeneous at the scale posed by the THz wavelength. Thus, we applied the effective medium theory and introduced the refractive index and absorption coefficient to describe the THz wave–tissue interaction, as well as to compare different classes of tissues, as shown in Fig. 2. This approach is widely applied in THz biophotonics, providing a simple way for processing and analyzing the THz-pulsed spectroscopy data.<sup>12</sup>

Nevertheless, several recent studies revealed inhomogeneous character of tissues, which could lead to the Mie scattering of THz waves,<sup>16,26,27,30</sup> making the effective medium theory to be rather controversial in many applications, and pushing further developments in THz biophotonics into the realm of analyzing the scattering properties of tissues. In our opinion, in this case, the radiative transfer theory might form a basis for further understanding the THz wave–tissue interaction.<sup>31</sup> Particularly, it could be used for better understanding of the THz response of inhomogeneous tissues of the brain, such as a perifocal region and other spatially inhomogeneous tissues of a tumor (for example, the tissues of glioma grade IV with necrotic debris), as well as brain tissues with a traumatic injury.<sup>28,29</sup> A comprehensive study of THz wave interaction with spatially inhomogeneous tissues is a promising topic for further research work.

In conclusion, we have studied the frequency-dependent THz optical properties of gelatin-embedded human brain gliomas of different WHO grade in order to analyze capabilities of THz technology in the intraoperative neurodiagnosis. The observed results of preliminary study of tissues *ex vivo* allowed us to objectively uncover strengths of THz technology in the intraoperative diagnosis of human brain gliomas of different WHO grades before committing to a full-blown study of tissues *in vivo*.

### Disclosures

The authors have no relevant financial interests in this article and no potential conflicts of interest to disclose.

### Acknowledgments

THz measurements and processing of the experimental data by K.M. Malakhov, S.-I.T. Beshplav, P.V. Nikitin, G.R. Musina, O.P. Cherkasova, and G.A. Komandin were supported by the grant from the Russian Science Foundation (RSF), Project #18–12–00328. Development of the tissue fixation procedure and the THz data processing methods, as well as fixation, transportation, and histological analysis of tissues by N.V. Chernomyrdin, I.N. Dolganova, A.V. Kosyrkova, I.V. Reshetov, A.A. Potapov, and K.I. Zaytsev were supported by the grants from the Russian Foundation for Basic Research (RFBR), Projects # 18-38-00504 and # 18-38-00853.

### References

- Q. Ostrom et al., “CBTRUS statistical report: primary brain and other central nervous system tumors diagnosed in the united states in 2011–2015,” *Neuro-Oncology* **20**(Suppl. 4), iv1–iv86 (2018).
- R. Stupp et al., “Radiotherapy plus concomitant and adjuvant temozolomide for glioblastoma,” *N. Engl. J. Med.* **352**(10), 987–996 (2005).
- E. Chang et al., “Multiinstitutional validation of the University of California at San Francisco low-grade glioma prognostic scoring system,” *J. Fla. Med. Assoc.* **111**(2), 203–210 (2009).
- M. Hefli et al., “Fluorescence-guided surgery for malignant glioma: a review on aminolevulinic acid induced protoporphyrin IX photodynamic diagnostic in brain tumors,” *Curr. Med. Imaging Rev.* **6**(4), 254–258 (2010).
- T. Garzon-Muvdi et al., “Intraoperative imaging techniques for glioma surgery,” *Future Oncol.* **13**(19), 1731–1745 (2017).
- B. Schatlo et al., “Outcomes after combined use of intraoperative MRI and 5-aminolevulinic acid in high-grade glioma surgery,” *Neuro-Oncology* **17**(12), 1560–1567 (2015).
- N. Pustogarov et al., “Hiding in the shadows: CPOX expression and 5-ALA induced fluorescence in human glioma cells,” *Mol. Neurobiol.* **54**(7), 5699–5708 (2017).
- B. Chen et al., “Gross total resection of glioma with the intraoperative fluorescence-guidance of fluorescein sodium,” *Int. J. Med. Sci.* **9**(8), 708–714 (2012).
- D. Orringer et al., “Rapid intraoperative histology of unprocessed surgical specimens via fibre-laser-based stimulated Raman scattering microscopy,” *Nat. Biomed. Eng.* **1**, 0027 (2017).
- M. Kircher et al., “A brain tumor molecular imaging strategy using a new triple-modality MRI-photoacoustic-Raman nanoparticle,” *Nat. Med.* **18**, 829–834 (2012).
- F. Vasefi et al., “Review of the potential of optical technologies for cancer diagnosis in neurosurgery: a step toward intraoperative neurophotonics,” *Neurophotonics* **4**(1), 011010 (2016).
- O. Smolyanskaya et al., “Terahertz biophotonics as a tool for studies of dielectric and spectral properties of biological tissues and liquids,” *Prog. Quantum Electron.* **62**, 1–77 (2018).
- S. Lepeshov et al., “Enhancement of terahertz photoconductive antenna operation by optical nanoantennas,” *Laser Photonics Rev.* **11**(1), 1600199 (2017).
- H. Guerboukha, K. Nallappan, and M. Skorobogatiy, “Toward real-time terahertz imaging,” *Adv. Opt. Photonics* **10**(4), 843–938 (2018).
- E. Pickwell et al., “Simulation of terahertz pulse propagation in biological systems,” *Appl. Phys. Lett.* **84**(12), 2190–2192 (2004).
- N. Chernomyrdin et al., “Reflection-mode continuous-wave 0.15λ-resolution terahertz solid immersion microscopy of soft biological tissues,” *Appl. Phys. Lett.* **113**(11), 111102 (2018).
- S. Oh et al., “Study of freshly excised brain tissues using terahertz imaging,” *Biomed. Opt. Express* **5**(8), 2837–2842 (2014).
- G. McIntyre, “Cell hydration as the primary factor in carcinogenesis: a unifying concept,” *Med. Hypotheses* **66**(3), 518–526 (2006).
- K. Meng et al., “Terahertz pulsed spectroscopy of paraffin-embedded brain glioma,” *J. Biomed. Opt.* **19**(7), 077001 (2014).
- S. Yamaguchi et al., “Brain tumor imaging of rat fresh tissue using terahertz spectroscopy,” *Sci. Rep.* **6**, 30124 (2016).
- Y. Ji et al., “Terahertz reflectometry imaging for low and high grade gliomas,” *Sci. Rep.* **6**, 36040 (2016).
- N. Chernomyrdin et al., “In vitro terahertz spectroscopy of gelatin-embedded human brain tumors: a pilot study,” *Proc. SPIE* **10716**, 107160S (2018).
- S. Fan et al., “Gelatin embedding: a novel way to preserve biological samples for terahertz imaging and spectroscopy,” *Phys. Med. Biol.* **60**(7), 2703–2713 (2015).
- G. Katyba et al., “Sapphire photonic crystal waveguides for terahertz sensing in aggressive environments,” *Adv. Opt. Mater.* **6**, 1800573 (2018).
- F. Harris, “On the use of windows for harmonic analysis with the discrete Fourier transform,” *Proc. IEEE* **66**(1), 51–83 (1978).
- C. Joseph et al., “Imaging of ex vivo nonmelanoma skin cancers in the optical and terahertz spectral regions. Optical and terahertz skin cancers imaging,” *J. Biophotonics* **7**(5), 295–303 (2014).
- B. Fan, V. Neel, and A. Yaroslavsky, “Multimodal imaging for nonmelanoma skin cancer margin delineation,” *Lasers Surg. Med.* **49**(3), 319–326 (2017).
- H. Zhao et al., “High-sensitivity terahertz imaging of traumatic brain injury in a rat model,” *J. Biomed. Opt.* **23**(3), 036015 (2018).
- J. Shi et al., “Automatic evaluation of traumatic brain injury based on terahertz imaging with machine learning,” *Opt. Express* **26**(5), 6371–6381 (2018).
- A. Yaroslavsky et al., “Delineating nonmelanoma skin cancer margins using terahertz and optical imaging,” *J. Biomed. Photonics Eng.* **3**(1), 010301 (2017).
- V. Tuchin, *Tissue Optics: Light Scattering Methods and Instruments for Medical Diagnosis*, 3rd edn., SPIE Press, Bellingham, Washington (2015).

Biographies of the authors are not available.